# Electron Spin Density on the Axial His Ligand of High-Spin and Low-Spin Nitrophorin 2 Probed by Heteronuclear NMR Spectroscopy

Luciano A. Abriata,[†,‡] María-Eugenia Zaballa,[†] Robert E. Berry,[§] Fei Yang,[§] Hongjun Zhang,[§] F. Ann Walker,*[,§] and Alejandro J. Vila*[,†]

[†]Instituto de Biología Molecular y Celular de Rosario (IBR-CONICET), Facultad de Ciencias Bioquímicas y Farmacéuticas, Universidad Nacional de Rosario, Ocampo y Esmeralda, Predio CONICET Rosario, Rosario 2000, Santa Fe, Argentina

[§]Department of Chemistry and Biochemistry, The University of Arizona, Tucson, Arizona 85721-0041, United States

Ⓢ Supporting Information

ABSTRACT: The electronic structure of heme proteins is exquisitely tuned by the interaction of the iron center with the axial ligands. NMR studies of paramagnetic heme systems have been focused on the heme signals, but signals from the axial ligands have been rather difficult to detect and assign. We report an extensive assignment of the ^{1}H, ^{13}C and ^{15}N resonances of the axial His ligand in the NO-carrying protein nitrophorin 2 (NP2) in the paramagnetic high-spin and low-spin forms, as well as in the diamagnetic NO complex. We find that the high-spin protein has σ spin delocalization to all atoms in the axial His57, which decreases in size as the number of bonds between Fe(III) and the atom in question increases, except that within the His57 imidazole ring the contact shifts are a balance between positive σ and negative π contributions. In contrast, the low-spin protein has π spin delocalization to all atoms of the imidazole ring. Our strategy, adequately combined with a selective residue labeling scheme, represents a straightforward characterization of the electron spin density in heme axial ligands.
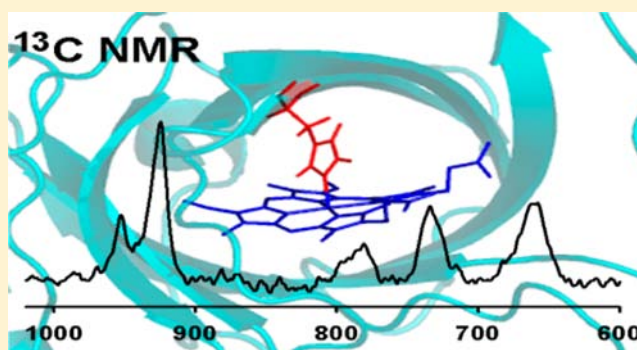
INTRODUCTION

The nitrophorins are a group of nitric oxide-carrying heme proteins found in the saliva of certain blood-sucking insects.[1] One such insect is *Rhodnius prolixus* (the "kissing bug"), which has a number of salivary nitrophorins that store NO via a ferriheme–nitrosyl complex and keep it stable for long periods of time.[2,3] Upon injection into the tissues of the bug's victim, dilution and pH elevation cause dissociation of NO. The NO diffuses through the tissues to the nearby capillaries to cause vasodilation (and inhibition of platelet aggregation), allowing more blood to be transported to the site of the wound.[4−6] In addition, the heme sites of the *Rhodnius* nitrophorins are able to bind histamine, which is released by mast cells and platelets of the victim in response to the wound. This histamine would otherwise cause swelling, itching, and the beginning of the immune response; its binding to the nitrophorins thus prevents the insect's detection for a period of time.[7] These two binding properties of the nitrophorins of the adult insect, named NP1−4 (in order of their decreasing abundances in the adult insect saliva), assist the bug in obtaining a sufficient blood meal.

The ligand-binding abilities of the heme iron of the nitrophorins are dictated by the heme group and the protein fold. Crystal structures of *Rhodnius* nitrophorins bound to various ligands have been reported for NP1,[8,9] NP2[10,55] and NP4.[11−13] These structures show the heme to be located inside, but at the open end of a β-barrel (Figure 1A), with the propionate groups protruding into the aqueous medium. This structure is unique for heme proteins, which more commonly have α-helical globin or 4-helix bundle folds.[14,15] The ferriheme prosthetic group is bound to the protein via a histidine ligand (His59 for NP1 and NP4, His57 for NP2 and NP3, detail for NP2 in Figure 1B), and the sixth coordination position is available to bind NO or other ligands. In the absence of exogenous ligands, this position is filled by a water molecule, yielding a weak ligand field that produces a high-spin, $S = 5/2$ state. Upon addition of ammonia, histamine or various imidazoles or cyanide ion to the solution, the added ligand binds with strong affinity (K_d values in the nanomolar or subnanomolar range)[16] producing low-spin, $S = 1/2$ derivatives. Notably, unlike most other heme proteins, nitrophorins form stable complexes in both Fe(III) and Fe(II) oxidation states with NO, the most important of which are the diamagnetic Fe(III)·NO complexes, with stabilities that facilitate release of NO upon dilution in human tissues or blood capillaries ($K_d \sim$ tens of nM to μM).[16] Ligand binding has been investigated by a number of techniques, most notably for this work, by NMR spectroscopy.[9,17−21]

NMR studies on the role of the axial histidine ligand in tuning the electronic structure of heme proteins have mainly
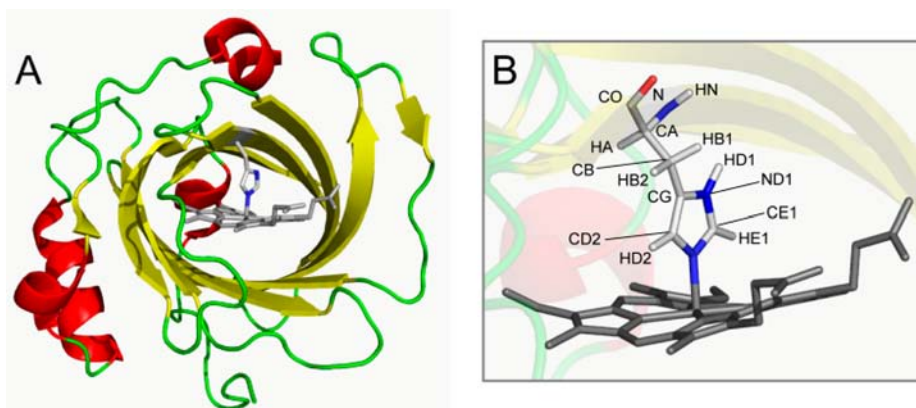
Figure 1. (A) Cartoon representation of the structure of NH_3-bound NP2 (PDB ID 2EU7) showing the heme group and His57 rendered as sticks. (B) Zoom on iron-bound His57, indicating the atom names used throughout this work. NP2 contains three additional histidines, His26, His119, and His138, all of which are on the outside surface of the β-barrel and do not interact with the heme. The figure was rendered with PyMol version 0.96 (DeLano Scientific).

focused on the resonances of the heme moiety[22,23] (see refs 22 and 23 and references therein), but NMR reports on the axial ligand itself are scarce,[24−26] since most of its ^1H resonances are severely broadened by the paramagnetic effect of the high-spin iron. In 1984 Moore and Williams assigned the His β-CH_2 and α-CH protons of tuna ferricytochrome c, a low-spin ferriheme protein.[27] The utilization of cyanide derivatives leading to low-spin species with longer nuclear relaxation times facilitated signal detection and assignment of several types of ferriheme proteins. In 1987 La Mar et al. assigned the His β-CH_2 and α-CH protons of the cyanide complex of horseradish peroxidase (HRPCN).[28] In 1988−1990, Emerson and La Mar assigned all of the His93 protons of sperm whale met-MbCN.[29−31] In 1992, Banci et al. investigated the ^1H resonances of the manganese peroxidase cyanide complex from *Phanerochaete chrysosporium* and compared the chemical shift of the histidine imidazole HD1 to those of other cyanide complexes of peroxidases.[32]

Most recently, Caillet-Saguy et al. were able to detect ^{15}N and ^{13}C resonances from the axial ligand in the Fe(III) hemophore from *Serratia marcescens*, HasA, which has a His-Tyr ligand set that exists in fast exchange on the ^1H chemical shift time scale as a $S = 5/2 \rightleftharpoons 1/2$ spin equilibrium, and to assign the three imidazole carbons of the histidine ligand in the Y75A mutant of that protein.[33−35]

In this work we make use of heteronuclear NMR spectroscopy, where the lower sensitivity of the heteronuclei to the paramagnetic effect of the metal center facilitates signal detection and assignment,[36−39] to investigate the ^1H, ^{13}C and ^{15}N resonances from the axial ligand of NP2, His57 (Figure 1B), in its three biologically relevant spin states ($S = 0$, 1/2, 5/2). We also present here the approach followed by us to obtain the NP2 protein selectively labeled with $^{13}C_6$,$^{15}N_3$-histidine.

■ EXPERIMENTAL SECTION

Preparation of the $^{13}C_6$,$^{15}N_3$-Histidine-Enriched NP2 Protein. Except where indicated, materials were obtained from Sigma-Aldrich and used without further purification. The expression and purification of native N-terminus NP2 (with native N- and C-termini) has been described elsewhere,[40] without the M0 residue resulting from the start codon being present, with the native D1 present as the first amino acid, and with no His$_6$-tag added for ease of purification. This construction allows the A-B and G-H loops of the protein to take up their native conformations. Hereafter in this paper we will usually refer to this protein simply as NP2. The NP2 expression plasmid[40] in pET-

26b (Novagen) was transformed into *ArcticExpress* (DE3) *Escherichia coli* cells (Stratagene), and grown overnight at 37 °C on LB agar plates containing kanamycin antibiotic for selection. A number of colonies were selected and each used to inoculate 1 mL of LB (containing kanamycin and gentamicin for antibiotic selection, 100 and 20 μg/mL, respectively). After 5 h at 37 °C in a shaker-incubator, 50 μL of the most cloudy growth was used to inoculate 50 mL of LB (also containing kanamycin and gentamicin), which was then grown at 37 °C in a shaker-incubator overnight. Twenty milliliters of the overnight culture was then used to inoculate each liter of initial rich defined growth medium, summarized in Supporting Information Table S1, and 100 μg/mL kanamycin was added for antibiotic selection. This was grown at 30 °C in a shaker-incubator (235 rpm) until an $OD_{600\ nm}$ of 0.8 was reached (4−5 h), before being cooled to ∼12 °C. The *E. coli* cells were collected by gentle centrifugation (1400g for ∼3 min), and the cells from 2 L of growth were resuspended in 1 L of final rich defined growth medium, also summarized in Supporting Information Table S1. This was grown at 12.5 °C in a shaker-incubator (235 rpm). After 15 min 0.23 mM L-histidine-$^{13}C_6$,$^{15}N_3$ hydrochloride mono-hydrate (98% isotopic enrichment, from Isotec) was added to the growth, along with 0.1 mM 5-aminolevulinic acid and 40 μM iron(II) sulfate. After 1 h NP2 expression was induced with 1 mM isopropyl β-D-1-thiogalactopyranoside. An additional 0.1 mM 5-aminolevulinic acid and 40 μM iron(II) sulfate were added after 2 and again after 4 days of growth. After 6 days the cells were harvested by centrifugation. The NP2 protein was isolated and purified as described elsewhere,[40] but included the addition of hemin during the purification to complex any apo-NP2 that might be present (0.2 mL of ∼2 mM hemin dissolved in a few drops of DMSO and diluted into pH 7.5 sodium phosphate buffer). A preliminary ^1H,^{15}N-HSQC spectrum, recorded at pH 5.0 and 298 K, showed that there were only three amide ^1H,^{15}N cross peaks in the normal protein amide window (5.5−11.0 ppm ^1H, 110−140 ppm ^{15}N) even down to the noise floor, and one additional amide cross peak, at 2.90 ^1H, 116.0 ^{15}N ppm, which confirmed that there was no measurable scrambling of the ^{15}N (and, by implication, the ^{13}C) label. Because of the limited size of the labeled sample, mass spectrometric analysis was not carried out. Any unlabeled histidine present in the protein sample would not interfere with the multidimensional NMR experiments carried out. The purified $^{13}C_6$,$^{15}N_3$-histidine-enriched NP2 (yielding ∼4 mg/L growth) was lyophilized and used to prepare the NMR samples.

Nuclear Magnetic Resonance Spectroscopy. All protein samples investigated were of the $^{13}C_6$,$^{15}N_3$-histidine-enriched NP2, which contained four $^{13}C_6$,$^{15}N_3$-His residues per protein molecule, i.e., His26, His57, His119, and His138, of which His57 is the protein-provided heme ligand. The other three His residues are on the outside of the β-barrel, far from the heme iron, and their resonances were all very similar in chemical shift, and were not assigned in detail. Three

axial ligands were used to create the desired iron spin states: H_2O (which, in the absence of any added ligand, binds to Fe(III) to yield a mainly high-spin, $S = 5/2$ state); N-methylimidazole (NMeIm, which binds to Fe(III) to yield a low-spin, $S = 1/2$ state, but does not bind incredibly tightly $(K_{eq} \sim 10^5 \ M^{-1})$, so that saturation transfer experiments can easily be used to connect resonances of the NMeIm complex to those of the high-spin complex to allow assignment of the high-spin resonances); and NO (which binds to Fe(III) to yield a diamagnetic, $S = 0$ state); none of these axial ligands was isotopically labeled. Protein samples were concentrated to ca. 1 mM in 50 mM sodium acetate buffer at pH 5.0. NMR experiments were carried out on a Bruker Avance II spectrometer operating at 600.13 MHz (^{1}H frequency), at 305 K. ^{1}H-detected spectra were acquired with a triple-resonance (TXI) probehead using the 1D PASE scheme[41] for suppression of water and diamagnetic signals, on spectral windows up to 120 kHz, and with total recycle times of ca. 500 ms. ^{1}H,^{13}C- and ^{1}H,^{15}N-HMQC experiments were acquired on spectral widths of ca. 50 kHz in the ^{1}H dimension (1–2k points) and ca. 35 kHz in the indirect dimension (64–128 points). The delay for coherence transfer was set according to the shortest T_2 of the involved ^{1}H signals, i.e. about 0.3–1 ms, and the relaxation delay was set to ca. 160 ms. Several experiments were carried out with the frequency of the heteronuclei set at different offsets. Fast HNCA and HNCACB experiments (total recycle time of 650–850 ms) were performed to identify both the backbone NH and the α carbon of His57 in high- and low-spin NP2. Standard HNCACB and (HB)CB(CGCD)HD experiments were performed to assign His57 resonances in the NO-bound diamagnetic form of NP2.

^{13}C direct-detected spectra were acquired with a broadband observe (BBO) probehead tuned at the proper frequency, using an excitation pulse of 7.85 μs at 88.67 W. Inverse gated ^{1}H decoupling was applied during acquisition of ^{13}C spectra. Initially, the carrier frequencies were set at different offsets in search of shifted NMR signals. Further experiments were performed with the carrier frequencies at 800 or 100 ppm, depending on which signals were being studied at the moment. The spectral windows and delays also varied in each experiment, resulting in total recycle times in the 100–500 ms range. Saturation transfer difference experiments between ^{13}C resonances from the high- and low-spin forms of the protein were performed on samples containing ca. 50% of the protein bound to N-methylimidazole (obtained by stepwise titration with the ligand). Saturation difference spectra were acquired with 40 ms irradiation at a power of 700 mW and a total recycle time of ca. 100 ms.

Titrations. To form the low-spin species, N-methylimidazole (as pure liquid) was added stepwise to high-spin NP2. The high-spin sample was poured into an Eppendorf tube, the ligand added and mixed, and the sample put back into the NMR tube. Full formation of the low-spin species (followed by NMR) required the addition of 3 equiv of NMeIm.

To form the diamagnetic species, excess DETA−NO powder was added to low-spin NP2 in an Eppendorf tube and then transferred immediately into a Shigemi NMR tube. The release of NO from the DETA−NO adduct was evidenced by the slow formation of small bubbles that pushed the piston. Complete formation of the diamagnetic species took ca. 18 h; after this time, a volume of ca. 100 μL of NO gas had been generated between the liquid surface and the bottom face of the Shigemi piston.

Analysis of the Chemical Shifts of His57 Bound to Low- and High-Spin Ferrihemes. The observed chemical shift for a particular resonance in a paramagnetic system contains contributions from the diamagnetic, contact, and pseudocontact shifts:[42,43]

$$\delta^{obs} = \delta^{dia} + \delta^{con} + \delta^{pc} \tag{1}$$

where δ^{dia} is the chemical shift that the resonance would have if the system were diamagnetic, δ^{con} is the through-bond contact shift, and δ^{pc} is the through-space pseudocontact shift. The contact contribution is given by

$$\delta_{con} = \frac{A\langle g\rangle\mu_B S(S + 1)}{3\gamma_N \hbar k_B T} \tag{2}$$

where A is the hyperfine (electron−nucleus) coupling constant, which provides a description of the electron spin delocalization, γ_N is the magnetogyric ratio of the nucleus of interest, $\langle g\rangle$ is the average g value of the metal ion, S is its total spin, μ_B is the electron Bohr magneton, $\hbar$ is the Planck's constant divided by 2π, k_B is Boltzmann's constant, and T is the absolute temperature. After measurement or estimation of the pseudocontact and diamagnetic shifts, eqs 1 and 2 are used to obtain A.

In this study, the diamagnetic shifts were measured on the diamagnetic Fe(III)·NO complex of NP2, and the pseudocontact shifts were calculated as described below.

For the low-spin species, magnetic anisotropy is large and the pseudocontact shift is given by[42,43]

$$\delta^{pc} = \frac{1}{24\pi r^3}\{[2\chi_{xx} - (\chi_{xx} + \chi_{yy})](3\cos^2 \theta - 1) + 3(\chi_{xx} - \chi_{yy})\sin^2 \theta \cos 2\Omega\} \tag{3}$$

where r, θ, and Ω are the polar coordinates of the atom of interest. Because the principal values of the χ tensor may not have been measured by NMR techniques, and because they can also be expressed approximately as a function of the g values,[44,45]

$$\chi_{ii} = \mu_B^2 g_{ii}^2 S(S + 1)/3k_B T \tag{4}$$

where all variables are defined as in eq 2, the pseudocontact shifts can be approximately estimated from a knowledge of the structure of the protein and the EPR g values:[42,44−46]

$$\delta^{pc} = \frac{\mu_B^2 S(S + 1)}{18kTr^3}\{[2g_{xx}^2 - (g_{xx}^2 + g_{yy}^2)](3\cos^2 \theta - 1) + 3(g_{xx}^2 - g_{yy}^2)\sin^2 \theta \cos 2\Omega\} \tag{5}$$

where r, θ, and Ω are the polar coordinates of the nucleus of interest in the reference frame of the **g** tensor with components g_{xx}, g_{yy}, and g_{zz}, and all other variables are defined as in eq 2. The approximation of eq 4 is valid for systems with no ZFS and when the spin multiplet ground state is isolated from excited electronic states.[44,45] Therefore, this assumption works fairly well for low-spin Fe(III). Since the magnetic susceptibility tensor of NP2-NMeIm has not yet been measured by NMR methods, the pseudocontact shifts of this complex were estimated using eq 5 and the g values of NP2-NMeIm. Polar coordinates and pseudocontact shifts were calculated by using a program based on a graphical interface developed by LAA (available upon request). The structure of the D1A mutant of NP2 bound to NH_3 at pH 7 (PDB ID 2EU7) was used as a model for calculations of low-spin pseudocontact shifts. The x and y molecular axes are aligned to the Fe-NC (pyrrole II) and Fe-ND (pyrrole III) bonds, respectively, leaving the z-axis <1° from the Fe-NE2(His57) bond. The g_{xx} and g_{yy} components of the **g** tensor are in the xy molecular plane, 17.5° clockwise from the corresponding molecular axes. This angle was computed from the relative ^{1}H NMR shifts of the methyl groups of low-spin NP2 by utilizing the ShiftPatterns program and the principle of counter-rotation of the **g** tensor with rotation of the imidazole plane from the x-axis.[47] The utilized g values were $g_{zz} = 3.05$, $g_{yy} = 2.25$, $g_{xx} = 1.28$ (Supporting Information Figure S1).

For high-spin Fe(III) under axial symmetry, the pseudocontact shift is given by[42,46]

$$\delta^{pc} = -28\frac{\langle g\rangle^2 \mu_B^2 D}{9k^2 T^2 r^3}[(3\cos^2 \theta - 1)] \tag{6}$$

where D is the zero-field splitting constant of the iron when bound to a particular axial ligand (H_2O in this case), and the other variables are defined as above. Although early calculations of the pseudocontact shifts of high-spin Fe(III) porphyrins[48] used D values measured by far-infrared spectroscopic techniques, more recent works have determined

D for various high-spin ferriheme proteins from analysis of the pseudocontact shifts of backbone protein resonances of ferriheme proteins and the geometric factors calculated from the crystallographic coordinates, which were found to range from $D = 9.1$ to 15.3 cm^{-1}.[49−54] Since no assignments are available for nuclei other than the labeled His57 surrounding the heme site in high-spin NP2, we cannot determine the D value by applying this method. Thus, we employed the mean of the values reported for high-spin ferriheme proteins,[49−54] $D = 12.2$ cm^{-1} as a plausible D value. The $\langle g \rangle$ value expected for $^6A_1$ high-spin Fe(III) is 2.0, and this was adopted in agreement with previous reports.[49−54] The structure of the (M0)NP2 construct at pH 6.5 (PDB ID 2A3F[55]) was employed as a model for the calculation of pseudocontact shifts in high-spin NP2.

Calculation of the Molecular Orbitals in the Imidazole Ring. A system consisting of a neutral imidazole molecule was generated with GaussView 3.09 and optimized at the DFT-B3LYP/6-31G+ level using Gaussian 09,[56] reaching no imaginary frequencies. The molecular orbitals were then computed with GaussView 3.09 from the optimized wave function and plotted at an isosurface level of ±0.07.

■ RESULTS AND DISCUSSION

His-Specific Labeling. For simplicity, an auxotrophic mutant strain of *E. coli* might be used to express a protein labeled at a desired amino acid, to prevent scrambling of the supplemented ^{13}C/^{15}N enriched amino acid through the many metabolic pathways that convert one amino acid into another. However, acquiring a high-yielding strain of *E. coli* auxotrophic for the specific amino acid desired can be difficult. From a thermodynamic point of view, histidine is an energetically costly amino acid for *E. coli* to produce.[57] Thus we would not expect significant dilution of the ^{13}C/^{15}N enriched histidine supplement, whereas it would be energetically favorable for *E. coli* to metabolize histidine. From a kinetic point of view, to destroy the enriched histidine, *E. coli* would have to switch on the various metabolic pathways required to metabolize it, and these pathways can be inhibited. Glutamine, which is easily metabolized into other amino acids, has been successfully used to specifically label a protein without using an auxotrophic mutant strain by manipulating the product feedback loops of *E. coli*'s amino acid metabolic pathways.[58] This method involved using large excesses of nonlabeled amino acids to suppress amino acid interconversion (i.e., a very rich medium), and inhibitors for glutamate/glutamine interconversion. Using the same principles to suppress mixing of the isotopically enriched histidine, we have developed a protocol to specifically label the histidine residues in NP2. *E. coli* cells containing the NP2 expression plasmid were first grown to log phase in a defined growth medium which was deficient in histidine and contained all of the other amino acids at the relative abundance found in *E. coli*.[59,60] These log-phase *E. coli* cells were then resuspended in a smaller volume (to maximize final yield)[61] of a defined growth medium containing ^{13}C$_6$,^{15}N$_3$-enriched L-histidine and a very large excess of the other amino acids in the relative abundance found for NP2, as described in the Experimental Section.

Detection and Assignment of ^{1}H, ^{13}C, and ^{15}N Resonances of His57 in Ligand-Free, High-Spin NP2. NP2 in the absence of added ligand is bound to a water molecule at pH 6.5 and below,[8−13] and has been shown to be high-spin, $S = 5/2$, on the basis of EPR ($g_y = 5.94$, $g_x = 5.67$, and $g_z = 1.99$)[62] and Mössbauer spectroscopy ($\delta = 0.30 \pm 0.01$ mms^{-1}, $\Delta E_Q = 2.53 \pm 0.01$ mms^{-1})[63] at 4.2 K. However, the ^{1}H NMR spectrum of ligand-free NP2 at 305 K, Figure 2, top, shows that the proton chemical shifts of the heme methyls of

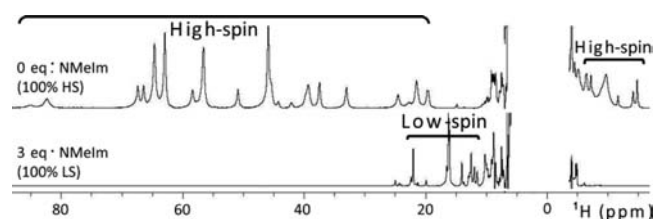**Figure 2.** 600 MHz ^{1}H NMR spectra of high-spin (top) and NMeIm-bound low-spin (bottom) NP2 in 50 mM sodium acetate, pH 5.0, at 305 K. FIDs were processed with a preexponential factor of 15 Hz. The assignments of all of the paramagnetically shifted ^{1}H resonances of the high-spin complex are well-known,[18] and are provided in Supporting Information Figure S3 (top). Those of the low-spin NMeIm complex are also well-known.[70].

the aqua complex of NP2 at ambient temperatures are smaller than those of the aqua complexes of metMb,[64,65] horseradish peroxidase (HRP),[66,67] other peroxidases,[32] inhibitor-bound heme oxygenase,[68,69] and bacterial ferricytochromes c'.[51,54] The smaller chemical shifts of NP2 may be attributed to an effect of heme ruffling, which is known to be very large in nitrophorins. Another possibility is the existence of a high-spin ⇌ low-spin equilibrium, as the one reported for HasA.[33−35] The possibility of this phenomenon is currently under investigation and will be addressed in a future manuscript (R.E.B. and F.A.W., to be submitted).

Figure 2 (top) also reveals two sets of resonances, consistent with the presence of two high-spin species in a ∼5:1 ratio. They correspond to the two orientations of the unsymmetrical protohemin molecule (termed **A** and **B** as defined previously,[18,19] Supporting Information Figure S2), which exchange slowly on the chemical shift time scale. (The $t_{1/2}$ is in the order of 5 h, but the heme orientation is essentially completely equilibrated by the time the protein exits the final size exclusion column at pH 5.0, after expression, export to the periplasm, isolation, and purification, a period of ∼2 weeks.) The major species corresponds to the **B** orientation, although the exact ratio varies with sample conditions according to our measurements (**A:B** ∼1:5 at 305 K and pH 5.0 in this work, as compared to **A:B** ∼ 1:12 at pH 7.0 and 298 K, Supporting Information Figure S3). Throughout this work we focus on the resonances arising from the major species, **B**, and all reported and discussed resonance assignments correspond to this form. Resonances from the minor **A** species always appear at similar chemical shifts to those of **B**.

The ^{13}C spectrum of ^{13}C,^{15}N-His-labeled high-spin NP2 (Figure 3A) shows a series of hyperfine-shifted resonances corresponding to these two high-spin species (**A** and **B**). Three major broad signals corresponding to the **B** species are observed between 1000 and 600 ppm (at 924, 734, and 658 ppm, Figure 3A, top). Several additional resonances can be identified within the diamagnetic region, three of them (located at 175.9, 140.7, and 79.7 ppm) displaying linewidths, T_1 values, and/or temperature dependences consistent with the paramagnetic effect of Fe(III) (Figure 3A, bottom). The large chemical shift values of the broad resonances shifted to lower shielding are due to large contact contributions, as discussed in detail below, and thus we attribute them to the three imidazole carbons of residue His57. Similar shifts to lower shielding (at 740 to 600 ppm) have been observed for the imidazole carbons of the histidine iron ligand in HasA.[33] The specific assignment of these resonances in NP2 is described later on on the basis of saturation transfer difference experiments that correlate them to
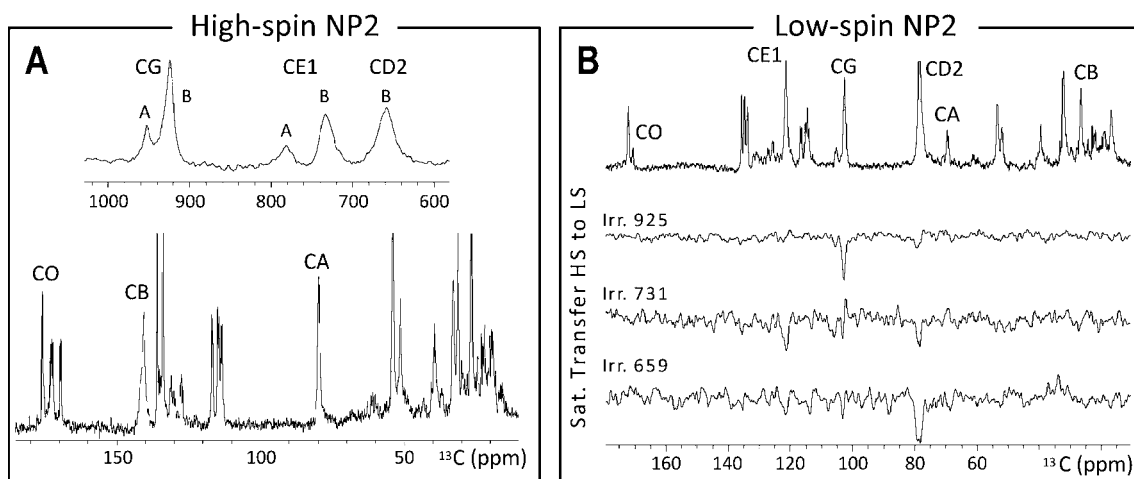
Figure 3. 150 MHz ^{13}C NMR spectra of high-spin (A) and low-spin (B) ^{13}C,^{15}N-His-labeled NP2 in 50 mM sodium acetate, pH 5.0, at 305 K. For spectra corresponding to the lower shielding and diamagnetic regions of the high-spin NP2, 400k and 20k transients were accumulated and were processed with preexponential factors of 400 and 20 Hz, respectively, whereas for the low-spin NP2 spectrum 20k transients were accumulated and processed with a preexponential factor of 20 Hz. Saturation transfer difference experiments were carried out on a sample containing both the high- and low-spin forms of the protein in a ca. 1:1 ratio and using a delay for transfer of 40 ms. For difference spectra shown here 120k transients were accumulated and processed with a preexponential factor of 100 Hz. Labels for His57 carbons (CE1, CD1, CG, CB, CA, etc.) are provided in Figure 1B. Labels (A, B) in panel A (top) correspond to the two different heme orientations.

the corresponding resonances of the low-spin NMeIm complex, as shown in Figure 3B, bottom.

The three paramagnetic resonances found within the diamagnetic ^{13}C chemical shift region were assigned by means of heteronuclear correlation experiments: ^{1}H,^{13}C-HMQC and HNCA (Figure 4). The ^{13}C resonance at 140.7

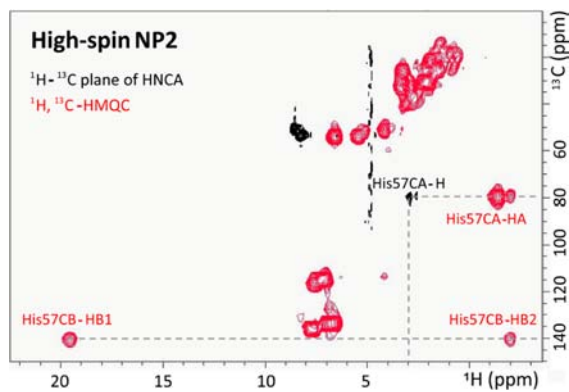**Figure 4.** ^{1}H–^{13}C-HMQC (red) and HNCA ^{1}H–^{13}C-plane (black) of high-spin NP2 in 50 mM sodium acetate, pH 5.0, at 305 K. The ^{1}H–^{13}C-HMQC spectrum was acquired with a total recycle time and a delay for transfer of 250 and 1 ms, respectively, and the ^{1}H–^{13}C-plane of the HNCA spectrum was acquired with a total recycle time of 700 ms. Cross peaks corresponding to His57 are labeled in the figure whereas the remaining cross peaks correspond to ^{1}H–^{13}C correlations of histidine residues other than His57 (i.e., His26, His119, and His138, not affected by the paramagnetism of the heme iron).

ppm shows correlations in the ^{1}H,^{13}C-HMQC spectrum with two proton resonances at 19.56 and −2.00 ppm. The latter resonances have been recently assigned by some of us to the HB1 (out of the imidazole plane) and HB2 (in the imidazole plane) protons of His57, respectively,[70] thus allowing us to assign the corresponding ^{13}C resonance to His57 CB. The carbon resonance at 79.7 ppm shows a correlation in the ^{1}H,^{13}C-HMQC, with a ^{1}H signal at −1.39 ppm, and a

correlation with an amide proton at 2.90 ppm in the ^{1}H,^{13}C plane of an HNCA experiment. Thus we unequivocally assign resonances at 79.7 ppm in ^{13}C and −1.39 and 2.90 ppm in ^{1}H to the CA, HA, and protein backbone amide HN nuclei of His57, respectively. Finally, the remaining ^{13}C resonance observed in the lower panel of Figure 3A, at 175.9 ppm, is assigned to the His57 carbonyl carbon.

It should be noted that the −1.39 ppm chemical shift value obtained here for the HA nucleus of His57 of native N-terminus NP2 at pH 5.0 differs from the 2.6 ppm value recently reported by some of us for the same nucleus of the closely related complex, NP2(D1A), based on its NOE correlation to the His57 HB1 proton in a sample prepared in ~100% D$_2$O at pH 7.0.[70] It is now clear that the assignment was incorrect; in fact, the resonance at 2.6 ppm in NP2(D1A) corresponds to the backbone amide HN proton of His57 (found for native N-terminus NP2 at 2.90 ppm in this work). The error arose from the observation that the signal was still detectable in a freshly made sample of NP2(D1A) in ~100% D$_2$O, probably due to its strong interaction with Phe66's backbone carbonyl through a hydrogen bond. Indeed, we have now observed that the mentioned response at 2.6 ppm in the previously reported WEFT-NOESY spectrum of NP2(D1A)[70] is vastly decreased in intensity when an equivalent spectrum was recorded after sixteen months of storage of a similar NP2(D1A) protein sample in ~100% D$_2$O at 4 °C, as shown in Supporting Information Figure S4. This is a clear example of how selective labeling and heteronuclear NMR experiments simplify spectral assignment.

The identification of His57 HA and HB resonances allows us to tentatively assign the broad solvent-exchangeable ^{1}H resonance at 82.3 ppm (Figure 2, top) to the imidazole HD1 proton of His57 on the basis of the NOEs observed between this signal and those of the HA and HB1 protons (located at 3.57 and 2.70 Å, respectively, from HD1) (Supporting Information Figure S5). The resonance corresponding to its bound N atom, ND1, could not be detected either in ^{15}N direct-detected 1D or in ^{1}H-detected HMQC spectra.

Resonances corresponding to the two carbon-bound protons in the imidazole ring of His57 of high-spin NP2 were also not detected for high-spin NP2. Consistent with our inability to detect these protons, we note that, for the analogous protons in high-spin horseradish peroxidase, La Mar and co-workers have estimated linewidths >10 kHz and T_1 values <0.1 ms.[67] Finally, the correlation between the His57 NH resonance at 2.90 ppm and a ^{15}N resonance at 116.0 ppm in a ^{1}H,^{15}N-HSQC spectrum leads to the assignment of this ^{15}N resonance to the protein backbone N nucleus of His57 (Supporting Information Figure S9).

Titration of Ligand-Free, High-Spin NP2 with *N*-Methylimidazole. Binding of NMeIm to the ferriheme iron produces a low-spin complex, as evidenced by the detection of ^{1}H resonances typical of low-spin ferriheme centers (Figure 2, bottom). The addition of NMeIm was also followed in the 1D ^{13}C spectra. During the titration, the intensity of all signals from the high-spin species decreased, with the concomitant rise of six new resonances in the diamagnetic region (Figure 3B, top). No new signals were detected outside this region. All the observed new resonances displayed strong temperature dependences, confirming that they arise from nuclei close to the paramagnetic iron ion.

Binding and release of NMeIm to/from NP2 under the conditions used in this work is slow on the chemical shift time scale, thus allowing us to perform saturation transfer experiments in a sample containing both the low-spin and high-spin species. Saturation transfer difference spectra of ^{13}C were acquired by irradiating the signals of high-spin NP2 at 924, 734, and 658 ppm, which elicited responses at 102.5, 121.4, and 80.6 ppm, respectively (Figure 3B, bottom). All these resonances were assigned to the specific imidazole carbons in a pure low-spin sample, as discussed below, and the obtained assignments were later on transferred to the corresponding resonances in the high-spin species.

Detection and Assignment of ^{1}H, ^{13}C, and ^{15}N Resonances of His57 in *N*-Methylimidazole-Bound, Low-Spin NP2. Following the approach used for high-spin NP2, the ^{1}H–^{13}C plane of an HNCA experiment of low-spin NP2 (Figure 5) shows a correlation between a ^{13}C resonance at 69.5 ppm and an HN at 10.10 ppm, allowing us to assign these two signals to the CA and HN nuclei of His57. Besides, a ^{1}H,^{13}C-HMQC spectrum of this sample (Figure 5) shows a cross peak between the His57 CA resonance and a proton at 8.01 ppm, assigned then as His57 HA. In the same HMQC spectrum, a carbon resonance at 16.9 ppm gives correlations with two proton resonances at 12.76 and 5.77 ppm, consistent with the pattern of His57 CB and its two attached HB1 and HB2 protons, respectively (following the stereospecific assignment by Shokhireva and Walker[70]). Our assignments, based on scalar correlations, confirm the assignments of the CA, CB, HA, HB1, and HB2 nuclei of His57 in low-spin NP2(D1A) recently reported by some of us on the basis of ^{1}H–^{1}H NOEs.[70]

The ^{1}H,^{13}C-HMQC spectrum from Figure 5 does not show any correlation that could be assigned to one-bond ^{1}H–^{13}C couplings from the imidazole ring. On the contrary, a ^{1}H,^{13}C-HMQC spectrum acquired with a very short coherence transfer delay (0.3 ms instead of 1 ms, Supporting Information Figure S7) revealed additional cross peaks correlating two ^{1}H resonances (at 9.30 and −4.29 ppm) with two ^{13}C resonances at 80.6 and 121.4 ppm, assigned to His57 imidazole carbons from the saturation transfer experiments previously described
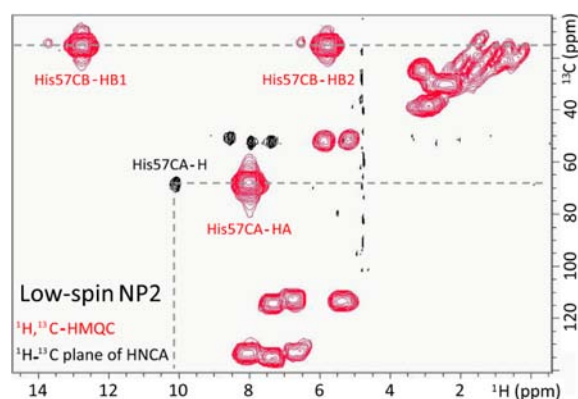

Figure 5. ^{1}H–^{13}C-HMQC (red) and HNCA plane (black) of low-spin NP2 in 50 mM sodium acetate, pH 5.0, at 305 K. The ^{1}H–^{13}C-HMQC spectrum was acquired with a total recycle time and a delay for transfer of 250 and 1 ms, respectively, and the ^{1}H–^{13}C-plane of the HNCA spectrum was acquired with a total recycle time of 700 ms. The two small HMQC cross peaks at larger ^{1}H chemical shift than the two His57CB-HB cross peaks are those arising from the **A** heme orientation. Cross peaks corresponding to His57 are labeled in the figure whereas the remaining cross peaks correspond to ^{1}H–^{13}C correlations of histidine residues other than His57.

(Figure 3B, bottom). It has been reported that low-spin heme systems present a typical higher/lower shielding pattern for their carbon-bound ^{1}H imidazole signals.[71−73] Taking this pattern into account, we assign the observed ^{1}H resonances at 9.30 and −4.29 ppm and ^{13}C resonances at 80.6 and 121.4 ppm to the HD2 and HE1 protons and CD2 and CE1 carbons of His57 in low-spin NP2, respectively. Furthermore, the saturation transfer experiments, shown in Figure 3B bottom, allow us to extend these assignments to the high-spin form, i.e., ^{13}C resonances at 658 and 734 ppm corresponding to CD2 and CE1 imidazole carbons in high-spin NP2, respectively. The remaining imidazole ^{13}C resonances in the low- and high-spin proteins (102.5 and 924 ppm, respectively) are then assigned to the quaternary His57 CG. Finally, the His57 CO resonance in low-spin NP2 was identified inside the diamagnetic region for carbonyls (at 170.7 ppm) as the one with increasing intensity during the titration with *N*-methylimidazole.

Backbone and imidazole nitrogens in low-spin NP2 were identified and assigned from a standard ^{1}H,^{15}N-HSQC experiment. This spectrum (Supporting Information Figure S6) shows seven strong NH correlations. Five of them can be safely attributed to the three diamagnetic histidines in NP2 (three backbone and two imidazole NH correlations), as their positions are barely affected relative to the high-spin form and their shifts are within the expected ranges for diamagnetic resonances. Of the two remaining cross peaks, the one at (127.6, 10.10) ppm is assigned to the backbone NH of His57 in low-spin NP2, based on its correlation with the His57 CA in the HNCA spectrum (Figure 5). We propose that the remaining cross peak, at 149.7 ppm in ^{15}N and 10.04 ppm in ^{1}H, corresponds to the imidazole ND1−HD1 pair of His57, considering its short T_1 value as well as its absence in the corresponding spectrum of high-spin NP2.

Detection and Assignment of ^{1}H, ^{13}C, and ^{15}N Resonances of His57 in NO-Bound, Diamagnetic NP2. A diamagnetic derivative of NP2 was prepared by adding excess NO (in the form of the DETA−NO adduct) to the *N*-methylimidazole-bound, low-spin species. This reaction is

favored by the tighter binding of NO to NP2 $(4 \times 10^7 \text{ M}^{-1})^{16}$ with respect to NMeIm ($\sim 10^5 \text{ M}^{-1}$, estimated). Addition of the odd-electron NO ligand to the d^5 Fe(III) center renders the system diamagnetic. The reaction between NMeIm-bound NP2 and NO was followed by ^{1}H NMR spectra, where all paramagnetically shifted signals decreased in intensity until they disappeared, indicating completion of the reaction.

The ^{1}H,^{15}N-HSQC spectrum of NO-bound NP2 in the backbone amides' region shows three cross peaks close to those from the diamagnetic His residues in the low- and high-spin forms, whereas the backbone ^{1}H–^{15}N cross peak from His57 moved to (6.37, 123.0 ppm) (Supporting Information Figure S9). An additional cross peak accounts for the correlation between His57's HD1 and ND1 at (10.48, 170.6 ppm). The backbone ^{15}N and ^{1}H resonances of His57 were correlated to the corresponding CA and CB nuclei via a 2D version of the triple-resonance experiment HNCACB without evolution of ^{15}N chemical shifts (Figure 6), which revealed chemical shifts of
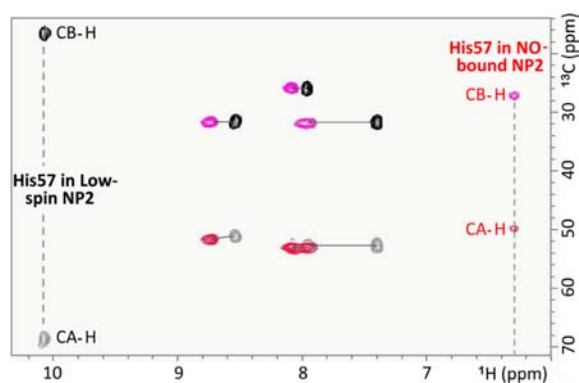

Figure 6. ^{1}H,^{13}C HNCACB planes (^{15}N chemical shift not evolved) of low-spin (black and gray contours) and NO-bound (magenta and red contours) NP2 in 50 mM sodium acetate, pH 5.0, at 305 K. Cross peaks corresponding to His57 are labeled in the figure whereas the remaining cross peaks correspond to ^{1}H–^{13}C correlations of histidine residues other than His57.

50.6 and 27.2 ppm, respectively. In a (HB)CB(CGCD)HD spectrum (Supporting Information Figure S9) the His57 CB resonance correlates with that of its HD2 proton at −0.63 ppm, which further correlates with its CD2 resonance at 118.6 ppm in a ^{1}H,^{13}C-HMQC spectrum of NO-bound NP2 (Figure 7).
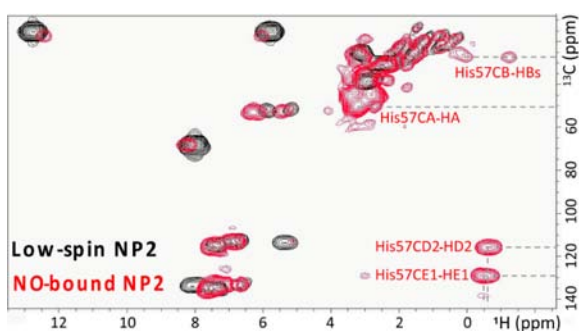

Figure 7. ^{1}H–^{13}C-HMQC spectra of low-spin (black) and NO-bound (red) NP2 in 50 mM sodium acetate, pH 5.0, at 305 K, acquired with a total recycle time and a delay for transfer of 250 and 1 ms, respectively. In the NO-bound NP2 spectrum, cross peaks corresponding to His57 are labeled in the figure whereas the remaining cross peaks correspond to ^{1}H–^{13}C correlations of histidine residues other than His57.

From this spectrum it is also possible to assign resonances corresponding to His57 HA (at 3.26 ppm, connected to the assigned CA resonance) and both His57 HB protons (at 0.08 and −1.25 ppm, connected to the assigned CB). The cross peak at (129.6, −0.52) ppm, present only in the ^{1}H,^{13}C-HMQC of NO-bound NP2, is assigned to the His57's CE1–HE1 correlation by comparison with the chemical shifts values observed for the CD2–HD2 correlation in this species. The two quaternary carbons, CO and CG, in NO-bound NP2, were assigned to resonances at 168.4 and 123.5 ppm, respectively, by comparing the ^{13}C direct-detected 1D spectra of low-spin and diamagnetic NP2, where only signals from His57 were affected.

It should be pointed out that the strong shifts to higher shielding observed for His57 protons in the diamagnetic, NO-bound form of NP2 can be attributed to ring current effects. The signs of the ring-induced chemical shifts are consistent with their position inside the conical region where shifts to higher shielding are induced, as predicted from calculations and observed experimentally in diamagnetic porphyrins.[74−79] Notably, the ring-induced shifts for protons (calculated as the difference between observed shifts and the expected diamagnetic shifts for a histidine residue in a β-sheet) show a good correlation with the Fe−proton distances (Supporting Information Figure S10). This correlation is weak for carbon resonances, probably due to the larger intrinsic chemical shift dispersion of this nucleus within a given secondary structure element ($\sim$1.5 to 3 ppm vs 0.1 to 0.4 ppm for ^{1}H).[80]

Spin Density Mapping on the Axial His of High- and Low-Spin NP2. The assignment of almost all resonances from the axial His57 ligand of NP2 in its three biologically relevant spin states (high-spin, low-spin, and diamagnetic, Table 1) allows us to map the spin delocalization on this residue in the two paramagnetic species and to identify the mechanisms that generate it. We have calculated the hyperfine (electron−nucleus) coupling constant (A/h) for each nucleus of His57 in high- and low-spin NP2, after subtraction of the experimental diamagnetic shifts and the calculated pseudocontact contributions (eqs 1−6). The obtained A/h values are summarized in Table 1 and illustrated in Figure 8A. Both species display a large amount of spin density on the imidazole ring, which is poorly transmitted through the aliphatic bonds connecting CB, CA, and the other backbone nuclei, which show much smaller A/h values, as expected.

It should be noted that the present analysis is based on two main assumptions concerning the calculation of the pseudocontact contributions. First, we cannot rule out the possibility that His57 in solution adopts a conformation slightly different compared to the one observed in the crystal structure. Thus, use of the X-ray coordinates may lead to a slightly inaccurate estimation of the pseudocontact shift values. However, the general trend should not be altered. Second, in the calculation of the pseudocontact shifts we have used the magnetic data derived from the **g** tensor, instead of the χ tensor. Also, for the low-spin NP2-NMeIm species we have taken the z-axis to be along the His NE2-Fe vector, and have used the principle of counter-rotation of the **g** tensor with rotation of the His57 imidazole plane to determine the orientation of g_{xx} and g_{yy}.[47] In two seminal papers by Emerson and La Mar,[30,31] they used the magnetic anisotropies as predicted by Horrocks and Greenberg[44] for the study of metMb-CN in terms of off-axis binding of the cyanide ion, and fit the pseudocontact shifts of a number of amino acid side chains near the heme, to an approximate 15° off-axis tilt of the z-axis toward the *meso-δ* carbon, which

Table 1. Resonance Assignments, Pseudocontact (PC) and Contact Shifts, and A/h Values for ^{1}H, ^{13}C, and ^{15}N Nuclei of His57 in Low- and High-Spin NP2 in 50 mM Sodium Acetate, pH 5.0, at 305 K

	NO-bound	low-spin				high-spin			
nucleus	diamagnetic shift (ppm)	obsd (ppm)	PC (ppm)	contact (ppm)	A/h (MHz)	obsd (ppm)	PC (ppm)[a]	contact (ppm)[a]	A/h (MHz)[a]
CO	168.4	170.7	3.8	−1.5	−0.01	175.9	−5.2	12.7	0.11
CA	50.6	69.5	6.7	12.2	0.11	79.7	−9.5	38.6	0.34
CB	27.2	16.9	10.8	−21.1	−0.18	140.7	−15.2	128.7	1.13
CG	123.5	102.5	27.0	−48.0	−0.42	924	−38.6	839.1	7.35
CD2	118.6	80.6	61.9	−99.9	−0.87	658	−83.3	622.7	5.46
CE1	129.6	121.4	64.3	−72.5	−0.64	734	−86.6	691	6.06
N	123.0	127.6	5.6	−1.0	0.00	116.0	−8	1	0.004
ND1	170.6	149.7	27.9	−48.8	0.17	ND[b]	−39.7	ND	ND
H	6.37	10.10	4.56	−0.83	−0.03	2.90	−6.58	3.11	0.11
HA	3.26	8.01	6.78	−2.03	−0.07	−1.39	−9.42	4.77	0.17
HB1(oop)[c]	0.08/−1.25[d]	12.76	8.02	4.66 to 5.99[e]	0.17 to 0.21	19.56	−11.22	30.70 to 32.03[e]	1.08 to 1.12[e]
HB2(ip)[f]	0.08/−1.25[d]	5.77	8.63	−1.61 to 2.94[e]	−0.06 to 0.1	−2.00	−11.89	9.81 to 11.14[e]	0.34 to 0.39[e]
HD2	−0.63	9.30	31.17	−21.24	−0.74	ND	−31	ND	ND
HE1	−0.52	−4.29	31.50	−35.27	−1.23	ND	−29.48	ND	ND
HD1	10.48	10.04	10.82	−11.26	−0.39	82.30	−15.06	86.88	3.05

[a]Pseudocontact shifts in the high-spin form are approximate due to the use of an estimated value for D in eq 6 and the possible existence of a HS ⇌ LS equilibrium like that reported for HasA (see text). This extends to the calculated contact shift and hyperfine coupling constant. [b]ND = not detected/not determined. [c]oop = out of the imidazole plane. [d]Stereoselective assignment was not possible for these two protons in the diamagnetic form of NP2, hence the ranges of possible contact shifts and A/h values in each case are reported. [e]The differences in contact shift contributions obtained for HB1 and HB2 protons can be accounted for by considering their orientation relative to the imidazole plane of His57, as discussed in ref 70. [f]ip = in the imidazole plane.
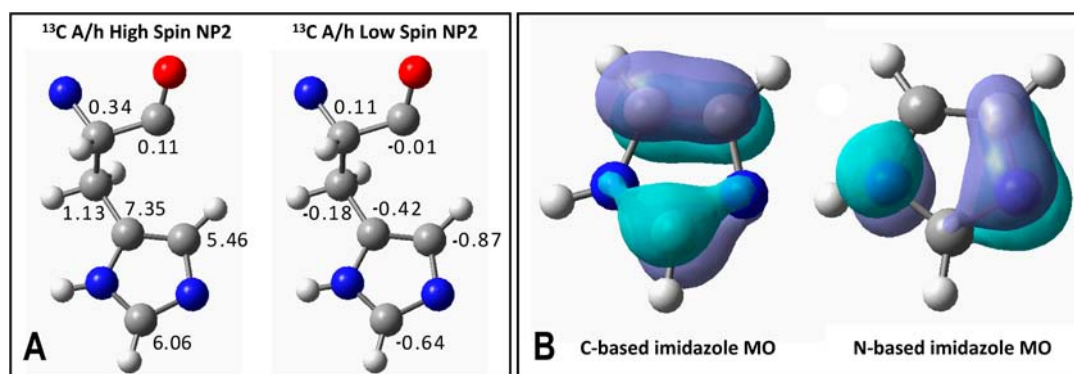

Figure 8. (A) A/h values for ^{13}C nuclei of His57 in high- and low-spin NP2 (values mapped from Table 1). (B) Carbon-based and nitrogen-based π molecular orbitals calculated for a free imidazole ring. Computation of these orbitals has been reported by Jones et al. obtaining comparable results to those shown here.[85]

coincided with the similar off-axis tilt of CO in the Mb-CO structure,[81] which was isostructural with metMb-CN.[31] This approach cannot be applied to the present case because of (1) the lack of a crystal structure for a NP-NMeIm complex and (2) the lack of assignments of protein resonances (others than those from His57) in the diamagnetic NO-bound form of NP2. We are aware that our results are only approximate, as off-axis tipping of the z-axis, if present, could be a major contributor to the pseudocontact shifts, and the accurate separation of observed shifts into pseudocontact and contact contributions is impossible without knowledge of the exact orientation of the z magnetic axis of the complex.

Based on the extensive study of the delocalization mechanisms observed for the two major paramagnetic spin states of Fe(III) porphyrins,[22,23] both model hemes and ferriheme proteins,[82] we should expect the imidazole ring portion of the histidine ligand to behave according to the same basic rules as observed for the macrocycle, i.e., that spin delocalization through σ-bonds (in the case of the axial ligands this is the electron in the d_{z^2} orbital of high-spin Fe(III)) leads to contact shifts to lower shielding (positive), which decrease in magnitude as the number of bonds between the metal and the nucleus of interest increases, whereas delocalization through π bonds (π-symmetry orbitals) leads to contact shifts to higher shielding (negative), which vary in size in proportion to the square of the orbital coefficient of that nucleus, and may thus not follow the same pattern of decrease as the number of bonds between the metal and the nucleus of interest increases.[83] Addition of an aliphatic carbon between the π system and the nucleus of interest causes reversal of the sign and decrease in the magnitude; this case is expected to occur in His57 for the CB, HB1, HB2, CA, HA, CO, N, and NH nuclei.

For the case of high-spin Fe(III) at 305 K, with $S = 5/2$ and one unpaired electron in each of the d-orbitals, both σ and π spin delocalization are possible, and their effects may at least partially cancel each other. Actually, since σ spin delocalization

is usually much greater than π for atoms only a few bonds from the metal, all contact shifts remain positive in sign, but may be attenuated because of the π contact shift contribution. The orbitals of Fe(III) which are relevant here are the d_{z^2} orbital, which can interact with the σ-symmetry orbital of the imidazole atom NE2, and the d_{yz} orbital, which can interact with the π system of atom NE2 of the imidazole ring of His57, specifically with one of the two imidazole ring π orbitals, most probably the one which has a large orbital coefficient at NE2. Quantum calculations were performed on a neutral imidazole molecule, as a simplified surrogate for a full system which would involve at least the heme group, its iron atom, and the whole histidine, and would require more sophisticated calculations. The two resulting π orbitals are one largely based on the carbon atoms and the other on the nitrogen atoms (Figure 8B). The σ-donor orbital of atom NE2 of the His57 imidazole ring will interact with the d_{z^2} orbital of Fe(III) by Im→Fe σ donation to the hole in the d_{z^2} orbital. The filled π orbital of atom NE2 will interact with the other atoms of the imidazole ring to create two π orbitals, the dominant one of which will interact with the d_{yz} orbital of Fe, again as an Im→Fe π donation, in this case to a π-symmetry hole in the d_{yz} orbital. It is this interaction that controls the spin delocalization to the porphyrin ring atoms of the ferriheme by controlling the orientation of the nodal plane of the ferriheme π system, and we have found in a large number of cases, for both high-spin[17] and low-spin[84] ferrihemes, that the orientation of the imidazole plane of the axial ligand(s) determines the pattern of spin delocalization in the porphyrin ring, as it must also in the imidazole ring of His57 itself.

For the high-spin complex, where the σ spin delocalization mechanism predicts positive contact shifts and A/h values, whereas the π spin delocalization mechanism predicts negative contact shifts and A/h values, we see that the observed value of A/h is large and positive at all three carbons of the imidazole ring, but is largest for the CG carbon, next largest for the CE1 carbon, and smallest for the CD2 carbon. Both CD2 and CE1 should have considerable σ spin delocalization possible, since they are both only two bonds from Fe, whereas CG should have somewhat less σ spin delocalization, since it is three (or four) bonds from Fe. According to the N-based π orbital shown in Figure 8B, in terms of π spin delocalization, CG should have the smallest π (negative) contact shift, whereas CD2 has the largest, and CE1 has an intermediate π negative contact shift. Assuming the σ spin density to be the major contributor, we would expect overall spin density to vary in the order CG > CE1 > CD2. However, if the C-based π orbital were used (Figure 8B, left), the π (negative) contact shift would be largest at CG, smallest at CD2, and intermediate at CE1. This would lead to overall spin density to vary in the order CE1, CD2 > CG. Thus, the observed A/h pattern is more compatible with the use of the nitrogen-based orbital rather than the carbon-based orbital. Unfortunately, the fact that the HD2 and HE1 resonances could not be detected for the high-spin complex means that they cannot help us in deciding which imidazole π orbital is used for spin delocalization.

For CB, CA, and CO of high-spin NP2, we see a decrease in size of the positive contact shift with each bond, with CB ~15% of CG, CA ~30% of CB, and CO ~30% of CA. This is consistent with σ spin delocalization. However, it seems that σ spin delocalization extends through more σ bonds than might have been expected.

Note that, in the case of high-spin NP2, the calculated pseudocontact shifts should be considered as approximate due to a possible spin equilibrium (see above) and the estimated value of D used in eq 6. Thus the tabulated contact shifts only represent the trend of the contact shifts for this spin state.

For the low-spin complex the situation is considerably clearer. The single unpaired electron is in a d_π orbital, usually taken to be d_{yz}. Thus, since the d_{z^2} orbital is empty, σ spin delocalization should be nil within the His57 imidazole ring and beyond. The π contact shift, of negative sign, should vary in the order CD2 > CE1 > CG if the nitrogen-based orbital is used, or the order CG > CD2 ~ CE1 if the carbon-based orbital is used. The observed order, in terms of magnitude (large negative spin density, A/h (−)), is CD2 > CE1 > CG, meaning that the orbital used for π spin delocalization is clearly the nitrogen-based orbital, as in the case of high-spin NP2.

For the aliphatic part of His57 in low-spin NP2, CB has negative spin density, which is smaller in size but of the same sign as that on CG. This is not the expected sign for the spin density of an aliphatic carbon bound to an aromatic ring which receives spin density from a metal.[22,23,82,83] Thus, there must be spin polarization at CB which is significant enough to switch the expected sign of the contact shift and A/h from (+) to (−).[86] CA has positive spin density, about half as much as the magnitude at CB, and the amount of spin density at CO is small enough to be within experimental error. As for spin polarization on atoms closer to Fe, indeed, the spin polarization contribution could increase in size as the number of bonds between Fe and the nucleus of interest decreases, but it cannot be evaluated in the presence of significant π spin delocalization.

Overall, the present strategy of selective amino acid labeling combined with the use of tailored heteronuclear NMR experiments provides a straightforward way of mapping the electron spin density of axial ligands in heme proteins. It allows us to probe much closer to the metal, with its unpaired electron(s), which raises the question of how to describe spin polarization in cases where π spin delocalization is expected and observed. Further experiments aimed at exploiting this technique to correlate these features with the strength of the iron−heme axial interaction are under way.

■ ASSOCIATED CONTENT

Ⓢ Supporting Information
A table describing the formulas of rich defined media employed (Table S1), an EPR spectrum of native N-terminus NP2 bound to NMeIm (Figure S1), scheme showing heme **A** and **B** orientations (Figure S2), pH dependence of ^{1}H NMR spectra of high-spin NP2 (Figure S3), comparison of the WEFT-NOESY spectra of NP2(D1A) obtained within a week after being dissolved in D_2O and after 16 months in D_2O (Figure S4), 1D NOE spectrum on His57 HD1 of high-spin NP2 (Figure S5), ^{1}H,^{15}N-HSQC spectra of high- and low-spin and NO-bound NP2 (Figures S6 and S8), slow and fast pulsing ^{1}H,^{13}C-HMQC spectra of low-spin NP2 (Figure S7), (HB)-CB(CGCD)HD spectrum of NO-bound NP2 (Figure S9) and correlations between ring-induced shifts and Fe-ligand distances (Figure S10). This material is available free of charge via the Internet at http://pubs.acs.org.

■ AUTHOR INFORMATION

Corresponding Author
*E-mail: vila@ibr-conicet.gov.ar (A.J.V.), awalker@email.arizona.edu (F.A.W.).

Author Contributions

The manuscript was written through contributions of all authors. All authors have given approval to the final version of the manuscript. L.A.A. and M.-E.Z. contributed equally to this work.

Notes

The authors declare no competing financial interest.

■ REFERENCES

(1) Walker, F. A. *J. Inorg. Biochem.* **2005**, *99*, 216.

(2) Walker, F. A.; Montfort, W. R. *Adv. Inorg. Chem.* **2000**, *51*, 295.

(3) Ribeiro, J. M.; Hazzard, J. M.; Nussenzveig, R. H.; Champagne, D. E.; Walker, F. A. *Science* **1993**, *260*, 539.

(4) Ribeiro, J. M.; Nussenzveig, R. H. *FEBS Lett.* **1993**, *330*, 165.

(5) Yuda, M.; Hirai, M.; Miura, K.; Matsumura, H.; Ando, K.; Chinzei, Y. *Eur. J. Biochem.* **1996**, *242*, 807.

(6) Nussenzveig, R. H.; Bentley, D. L.; Ribeiro, J. M. *J. Exp. Biol.* **1995**, *198*, 1093.

(7) Ribeiro, J. M.; Walker, F. A. *J. Exp. Med.* **1994**, *180*, 2251.

(8) Weichsel, A.; Andersen, J. F.; Champagne, D. E.; Walker, F. A.; Montfort, W. R. *Nat. Struct. Biol.* **1998**, *5*, 304.

(9) Ding, X. D.; Weichsel, A.; Andersen, J. F.; Shokhireva, T. K.; Balfour, C.; Pierik, A. J.; Averill, B. A.; Montfort, W. R.; Walker, F. A. *J. Am. Chem. Soc.* **1999**, *121*, 128.

(10) Andersen, J. F.; Montfort, W. R. *J. Biol. Chem.* **2000**, *275*, 30496.

(11) Andersen, J. F.; Weichsel, A.; Balfour, C. A.; Champagne, D. E.; Montfort, W. R. *Structure* **1998**, *6*, 1315.

(12) Weichsel, A.; Andersen, J. F.; Roberts, S. A.; Montfort, W. R. *Nat. Struct. Biol.* **2000**, *7*, 551.

(13) Roberts, S. A.; Weichsel, A.; Qiu, Y.; Shelnutt, J. A.; Walker, F. A.; Montfort, W. R. *Biochemistry* **2001**, *40*, 11327.

(14) Orengo, C. A.; Michie, A. D.; Jones, S.; Jones, D. T.; Swindells, M. B.; Thornton, J. M. *Structure* **1997**, *5*, 1093.

(15) Smith, L. J.; Kahraman, A.; Thornton, J. M. *Proteins* **2010**, *78*, 2349.

(16) Berry, R. E.; Ding, X. D.; Shokhireva, T.; Weichsel, A.; Montfort, W. R.; Walker, F. A. *J. Biol. Inorg. Chem.* **2004**, *9*, 135.

(17) Shokhireva, T.; Shokhirev, N. V.; Walker, F. A. *Biochemistry* **2003**, *42*, 679.

(18) Shokhireva, T.; Smith, K. M.; Berry, R. E.; Shokhirev, N. V.; Balfour, C. A.; Zhang, H.; Walker, F. A. *Inorg. Chem.* **2007**, *46*, 170.

(19) Shokhireva, T.; Weichsel, A.; Smith, K. M.; Berry, R. E.; Shokhirev, N. V.; Balfour, C. A.; Zhang, H.; Montfort, W. R.; Walker, F. A. *Inorg. Chem.* **2007**, *46*, 2041.

(20) Shokhireva, T. K.; Berry, R. E.; Zhang, H.; Shokhirev, N. V.; Walker, F. A. *Inorg. Chim. Acta* **2008**, *361*, 925.

(21) Berry, R. E.; Shokhireva, T.; Filippov, I.; Shokhirev, M. N.; Zhang, H.; Walker, F. A. *Biochemistry* **2007**, *46*, 6830.

(22) Walker, F. A. In *The Porphyrin Handbook*; Kadish, K. M., Smith, K. M., Guilard, R., Eds.; Academic Press: Boston, 2000; Vol. 5, p 81.

(23) La Mar, G. N.; Satterlee, J. D.; de Ropp, J. S. In *The Porphyrin Handbook*; Kadish, K. M., Smith, K. M., Guilard, R., Eds.; Academic Press: Boston, 2000; Vol. 5, p 185.

(24) Jackson, J. T.; La Mar, G. N.; Bartsch, R. G. *J. Biol. Chem.* **1983**, *258*, 1799.

(25) Thanabal, V.; de Ropp, J. S.; La Mar, G. N. *J. Am. Chem. Soc.* **1987**, *109*, 265.

(26) Qin, J.; La Mar, G. N.; Dou, Y.; Admiraal, S. J.; Ikeda-Saito, M. *J. Biol. Chem.* **1991**, *269*, 1083.

(27) Moore, G. R.; Williams, G. *Biochim. Biophys. Acta* **1984**, *788*, 147.

(28) Thanabal, V.; de Ropp, J. S.; La Mar, G. N. *J. Am. Chem. Soc.* **1987**, *109*, 7516.

(29) Emerson, S. D.; Lecomte, J. T. J.; La Mar, G. N. *J. Am. Chem. Soc.* **1988**, *110*, 4176.

(30) Emerson, S. D.; La Mar, G. *Biochemistry* **1990**, *29*, 1545.

(31) Emerson, S. D.; La Mar, G. N. *Biochemistry* **1990**, *29*, 1556.

(32) Banci, L.; Bertini, I.; Pease, E.; Tien, M.; Turano, P. *Biochemistry* **1992**, *31*, 10009.

(33) Caillet-Saguy, C.; Delepierre, M.; Lecroisey, A.; Bertini, I.; Piccioli, M.; Turano, P. *J. Am. Chem. Soc.* **2006**, *128*, 150.

(34) Caillet-Saguy, C.; Piccioli, M.; Turano, P.; Lukat-Rodgers, G.; Wolff, N.; Rodgers, K. R.; Izadi-Pruneyre, N.; Delepierre, M.; Lecroisey, A. *J. Biol. Chem.* **2012**, *287*, 26932.

(35) Caillet-Saguy, C.; Turano, P.; Piccioli, M.; Lukat-Rodgers, G. S.; Czjzek, M.; Guigliarelli, B.; Izadi-Pruneyre, N.; Rodgers, K. R.; Delepierre, M.; Lecroisey, A. *J. Biol. Chem.* **2008**, *283*, 5960.

(36) Machonkin, T. E.; Westler, W. M.; Markley, J. L. *Inorg.Chem* **2005**, *44*, 779.

(37) Bertini, I.; Luchinat, C.; Parigi, G.; Pierattelli, R. *Dalton Trans.* **2008**, 3782.

(38) Bertini, I.; Felli, I. C.; Luchinat, C.; Parigi, G.; Pierattelli, R. *ChemBioChem* **2007**, *8*, 1422.

(39) Abriata, L. A.; Ledesma, G. N.; Pierattelli, R.; Vila, A. J. *J. Am. Chem. Soc.* **2009**, *131*, 1939.

(40) Berry, R. E.; Muthu, D.; Shokhireva, T. K.; Garrett, S. A.; Zhang, H.; Walker, F. A. *Chem. Biodiversity* **2012**, *9*, 1739.

(41) Bondon, A.; Mouro, C. *J. Magn. Reson.* **1998**, *134*, 154.

(42) Kurland, R. J.; McGarvey, B. R. *J. Magn. Reson.* **1970**, *2*, 286.

(43) Banci, L.; Bertini, I.; Luchinat, C. *Nuclear and Electron Relaxation. The Magnetic Nucleus-Unpaired Electron Coupling in Solution*; VCH: Weinheim, 1991.

(44) Horrocks, W. D., Jr.; Greenberg, E. S. *Biochim. Biophys. Acta* **1973**, *322*, 382.

(45) Horrocks, W. D.; Greenberg, E. S. *Mol. Phys.* **1974**, *27*, 993.

(46) Bertini, I.; Luchinat, C. *NMR of Paramagnetic Molecules in Biological Systems*; Benjamin/Cummings: Menlo Park, CA, 1986.

(47) Shokhirev, N. V.; Walker, F. A. *J. Am. Chem. Soc.* **1998**, *120*, 981.

(48) La Mar, G. N.; Eaton, G. R.; Holm, R. H.; Walker, F. A. *J. Am. Chem. Soc.* **1973**, *95*, 63.

(49) Kao, Y. H.; Lecomte, J. T. J. *J. Am. Chem. Soc.* **1993**, *115*, 9754.

(50) Demene, H.; Tsan, P.; Gans, P.; Marion, D. *J. Phys. Chem. B* **2000**, *104*, 2559.

(51) Tsan, P.; Caffrey, M.; Lawson Daku, M.; Cusanovich, M. A.; Marion, D.; Gans, P. *J. Am. Chem. Soc.* **1999**, *121*, 1795.

(52) Ma, L.; Liu, Y.; Zhang, X.; Yoshida, T.; Langry, K. C.; Smith, K. M.; La Mar, G. N. *J. Am. Chem. Soc.* **2006**, *128*, 6391.

(53) Asokan, A.; de Ropp, J. S.; S.L., N.; Ortiz de Montellano, P. R.; La Mar, G. N. *J. Am. Chem. Soc.* **2001**, *123*, 4243.

(54) Clark, K.; Laxmichand, B. D.; Bartsch, R. G.; Cusanovich, M. A.; La Mar, G. N. *J. Am. Chem. Soc.* **1996**, *118*, 4654.

(55) Weichsel, A.; Berry, R. E.; Zhang, H.; Walker, F. A.; Montfort, W. R. PDB files available (http://www.rcsb.org/): 1PEE, 1PM1, 1T68, 2A3F, 2ACP, 2AH7, 2AL0, 2ALL, 2AMM, 2ASN, 2EU7, 2HYS, 2GTF.

(56) Frisch, M. J.; Trucks, G. W.; Schlegel, H. B.; et al. *Gaussian 09, Revision A.02*; Gaussian, Inc.: Wallingford, CT, 2009.

(57) Akashi, H.; Gojobori, T. *Proc. Natl. Acad. Sci. U.S.A.* **2002**, *99*, 3695.

(58) Tong, K. I.; Yamamoto, M.; Tanaka, T. *J. Biomol. NMR* **2008**, *42*, 59.

(59) Söll, D. *tRNA: Structure, Biosynthesis and Function*; ASM Press: Washington, DC, 1995.

(60) Neidhardt, F. C. *Escherichia coli and Salmonella typhimurium: Cellular and Molecular Biology*; American Society for Microbiology: Washington, DC, 1987.

(61) Marley, J.; Lu, M.; Bracken, C. *J. Biomol. NMR* **2001**, *20*, 71.

(62) Singh, R.; Berry, R. E.; Yang, F.; Zhang, H.; Walker, F. A.; Ivancich, A. *Biochemistry* **2010**, *49*, 8857.

(63) Moeser, B.; Janoschka, A.; Wolny, J.; Filipov, I.; Chumakov, A. I.; Walker, F. A.; Schünemann, V. *Hyperfine Interact.* **2012**, *206*, 19.

(64) Lecomte, J. T. J.; Unger, S. W.; La Mar, G. N. *J. Magn. Reson.* **1991**, *94*, 112.

(65) Yamamoto, Y.; Chujo, R.; Inoue, Y.; Suzuki, T. *FEBS Lett.* **1992**, *310*, 71.

(66) Thanabal, V.; de Ropp, J. S.; La Mar, G. N. *J. Am. Chem. Soc.* **1987**, *109*, 265.

(67) de Ropp, J. S.; Mandal, P.; Brauer, S. L.; La Mar, G. N. *J. Am. Chem. Soc.* **1997**, *119*, 4732.

(68) Zeng, Y.; Caignan, G. A.; Bunce, R. A.; Rodríguez, J. C.; Wilks, A.; Rivera, M. *J. Am. Chem. Soc.* **2005**, *127*, 9794.

(69) Peng, D.; Ma, L.; Ogura, H.; Yang, E.; Zhang, X.; Yoshida, T.; La Mar, G. N. *Biochemistry* **2010**, *49*, 5832.

(70) Shokhireva, T. K.; Walker, F. A. *J. Biol. Inorg. Chem.* **2012**, *17*, 911.

(71) Satterlee, J. D.; La Mar, G. N. *J. Am. Chem. Soc.* **1976**, *98*, 2084.

(72) La Mar, G. N.; Frye, J. S.; Satterlee, J. D. *Biochim. Biophys. Acta* **1976**, *428*, 78.

(73) Bertini, I.; Turano, P.; Vila, A. *J. Chem. Rev.* **1993**, *93*, 2833.

(74) Abraham, R. J. *Mol. Phys.* **1961**, *4*, 145.

(75) Caughey, W. S.; Koski, W. S. *Biochemistry* **1962**, *1*, 923.

(76) Storm, C. B.; Corwin, A. H. *J. Org. Chem.* **1964**, *29*, 3700.

(77) Kane, A. R.; Valman, R. G.; Kenney, M. E. *Inorg. Chem.* **1968**, *7*, 2588.

(78) Juselius, J.; Sundholm, D. *J. Org. Chem.* **2000**, *65*, 5233.

(79) Iwamoto, H.; Hori, K.; Fukazawa, Y. *Tetrahedron Lett.* **2005**, *46*, 731.

(80) Avbelj, F.; Kocjan, D.; Baldwin, R. L. *Proc. Natl. Acad. Sci. U.S.A.* **2004**, *101*, 17394.

(81) Kuriyan, J.; Wilz, S.; Karplus, M.; Petsko, G. A. *J. Mol. Biol.* **1986**, *192*, 133.

(82) Walker, F. A. In *Handbook of Porphyrin Science*; Kadish, K. M., Smith, K. M., Guilard, R., Eds.; World Scientific: Hackensack, NJ, 2010; Vol. *VI*, p 1.

(83) Walker, F. A. *Inorg. Chem.* **2003**, *42*, 4526.

(84) Shokhirev, N. V.; Walker, F. A. *J. Biol. Inorg. Chem.* **1998**, *3*, 581.

(85) Jones, C. M.; Johnson, C. R.; Asher, S. A.; Shepherd, R. E. *J. Am. Chem. Soc.* **1985**, *107*, 3772.

(86) Bertini, I., Luchinat, C., Parigi, G. Solution NMR of Paramagnetic Molecules. In *Current Methods in Inorganic Chemistry*; Elsevier: Amsterdam, Netherlands, 2001; Vol. 2, p 55.

1295

dx.doi.org/10.1021/ic301805y | *Inorg. Chem.* 2013, 52, 1285−1295